

Luminescent Iridium(III) Complexes

Highly Luminescent Mono- and Dinuclear Cationic Iridium(III) Complexes Containing Phenanthroline-Based Ancillary Ligand

Xiao-Han Yang,^[a] Min Li,^[a] Hui Peng,^[a] Qian Zhang,^[a] Shui-Xing Wu,^[a] Wan-Qing Xiao,^[a] Xing-Liang Chen,^[a] Zhi-Gang Niu,^[b] Guang-Ying Chen,^[b] and Gao-Nan Li^{*[a]}

Abstract: A new family of mononuclear (**1–2**) and dinuclear (**3–5**) cationic iridium(III) complexes have been synthesized and fully characterized. These complexes contain 2-(4-(trifluoromethyl)phenyl)pyridine (cf_3ppy , **L1**) and 1-(4-(trifluoromethyl)phenyl)isoquinoline (cf_3piq , **L2**) as cyclometalating ligands, 1,10-phenanthroline (**LX-1**) as the ancillary ligand and 1,4-bis(1-phenyl-1H-imidazo[4,5-f][1,10]phenanthroline-2-yl)benzene (biphen, **LX-2**) as the bridging ligand. The crystal structure of **LX-2** has been determined by X-ray analysis. All of the com-

plexes are green-red emissive with quantum yields of 16.6–93.5 % and lifetimes of 1.66–2.89 μs in solution at room temperature. Density functional theory (DFT) calculations have been carried out to gain insight into the nature of the low-lying transitions and also to rationalize the electrochemical and photophysical properties. These research results reveal that the π -conjugation system of C^N ligands and the diiridium system with conjugated bridging ligand are both beneficial for the red-shift of the absorption and emission spectra.

Introduction

Iridium(III) complexes as phosphorescence emitters have been extensively employed in full-color organic light-emitting diode (OLED) displays and white light sources.^[1–3] This is due to their excellent luminescence properties,^[4,5] such as high quantum yields, long excited-state lifetimes, good thermal and photochemical stability, and facile emission color tunability.^[6,7] Particularly, cyclometalated heteroleptic and homoleptic mono-iridium complexes have been intensely studied over the past couple of decades.^[8–11] In contrast, cyclometalated diiridium complexes are rarely investigated, because they are usually more weakly emissive than mononuclear analogues and are, therefore, generally considered not suitable for OLEDs.^[12–14] However, recent research has found that judicious molecular design for diiridium complexes can overcome the above deficiency. For example, in 2014, Bryce and co-workers reported high-efficiency PhOLEDs of dinuclear iridium(III) emitters with external quantum efficiencies of 11 %.^[15] Subsequently, in 2016, Williams, Kozhevnikov and co-workers reported three very bright diiridium complexes with solution-state PLQYs of up to 100 %, measured using $\text{Ir}(\text{ppy})_3$ in 2-Me THF as the standard.^[16]

Accordingly, the study of phosphorescent diiridium complexes is a rapidly expanding topic based on the following pro-

spective advantages. Firstly, the variation of the bridging ligands within diiridium complexes can provide another tuning of photophysical properties in comparison to mono-iridium systems.^[17] Secondly, the rigid conjugated bridging ligands in dinuclear complexes can facilitate spin-orbit coupling, improve the radiative rate constant (k_r), and hence increase the phosphorescence efficiency, as required for use in organic light-emitting diodes.^[18,19] Thirdly, dinuclear complexes easier access to efficient red emitters through conjugated bridging ligands.^[20] For example, in 2014, Kozhevnikov and co-workers described the dinuclear Ir(III) complexes with rigid, bridged bis-terdentate cyclometalating ligands, which exhibited red emission with the quantum yield of 0.65.^[18] In 2016, Wong and co-workers reported two red-emitting dinuclear Ir(III) complexes with short conjugated bridging ligands, and the quantum yield is up to 0.61.^[21] Meanwhile, in a large number of cases, we also found that the emission bands of dinuclear complexes moved to longer wavelengths than the related mononuclear complexes,^[18,21,22] even reached to the deep-red region.^[23,24] This is because dinuclear complexes with π -extended ligands would allow a facilitating electron delocalization and thereby lead to a red-shifted emission.^[16,25]

Our group have been committed to exploring new red-emissive Ir(III) complexes with large quantum yields, for the realization of highly efficient WOLEDs.^[26–28] In general, the red emitters are designed by raising the HOMO level or lowering the LUMO level of the complex, aiming to reduce the energy gap.^[29] The approach is usually achieved by the introduction of an electron-donating group into the C^N ligand^[30] or extending π -conjugation of the C^N ligand.^[28] Herein, we chose $\text{cf}_3\text{ppy}/\text{cf}_3\text{piq}$ compounds as the C^N ligands and designed a π -conjugated compound (**LX-2**) as the bridging ligand to yield a series of dinuclear cyclometalated iridium(III) complexes (**3–5**). Spe-

[a] Key Laboratory of Electrochemical Energy Storage and Energy Conversion of Hainan Province, College of Chemistry and Chemical Engineering, Hainan Normal University, Haikou 571158, China
E-mail: ligaonan2008@163.com

[b] Key Laboratory of Tropical Medicinal Plant Chemistry of Ministry of Education, Hainan Normal University, Haikou 571158, China

Supporting information and ORCID(s) from the author(s) for this article are available on the WWW under <https://doi.org/10.1002/ejic.201801367>.

cially, we designed the different cyclometalated ligands in complex **4**, which would provide the possibility of dual photoluminescence originated from different lowest energy excited states. For comparative purposes, we also synthesised two corresponding cf_3ppy/cf_3piq -based mononuclear cyclometalated iridium(III) complexes containing phenanthroline ancillary ligand (**1–2**). The electrochemical properties of these complexes have been measured and analyzed. Their absorption spectra have been rationalized on the basis of density functional theory (DFT) and time-dependent DFT (TDDFT). Their luminescence properties have been investigated both in solution and in the solid state, where some of them are strongly emissive.

Results and Discussion

Synthesis and Characterization

Cyclometalated ligands **L1–L2**, ancillary ligand **LX-2** and their corresponding Ir(III) complexes **1–5** are synthesized and shown in Scheme 1 and Scheme 2. The ligands **L1** and **L2** were conveniently prepared via an efficient Suzuki coupling reaction with $Pd(dppf)Cl_2$ catalyst, which used 4-(trifluoromethyl)phenylboronic acid and the corresponding halogenated heterocyclic compounds 2-bromopyridine/1-chloroisoquinoline. The ancillary ligand **LX-2** was prepared through a multi-component cyclization reaction with terephthalaldehyde, aniline and 1,10-phenanthroline-5,6-dione.^[31] Cyclometalated Ir(III) dichloro-bridged dimers $[(C^{\wedge}N)_2Ir(\mu-Cl)]_2$ were synthesized by $IrCl_3 \cdot 3H_2O$ with cyclometalated ligands (2.2 equiv) in a 2:1 mixture of 2-ethoxyethanol and deionized water according to a similar method reported by Nonoyama.^[32] Then the new mononuclear and binuclear iridium(III) complexes **1–5** were obtained by the reaction of chloride-bridged dimer $[Ir(C^{\wedge}N)_2(\mu-Cl)]_2$ with ancillary ligands in $CH_2Cl_2/MeOH$ (1:1) followed by addition of excess NH_4PF_6 . All the desired products were characterized by 1H , ^{19}F and ^{31}P NMR spectroscopy, ESI-MS spectrometry and elemental analysis.

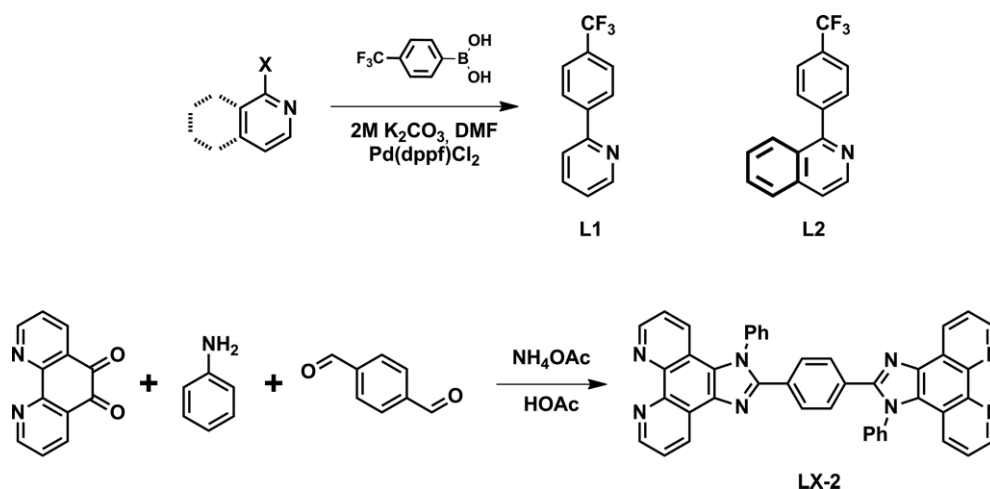
Structural Description

The crystal structure of **LX-2** was determined by X-ray diffraction, and the ORTEP diagram is shown in Figure 1a. The crystallographic data are given in Table S1; selected bond lengths and angles are collected in Table S2.

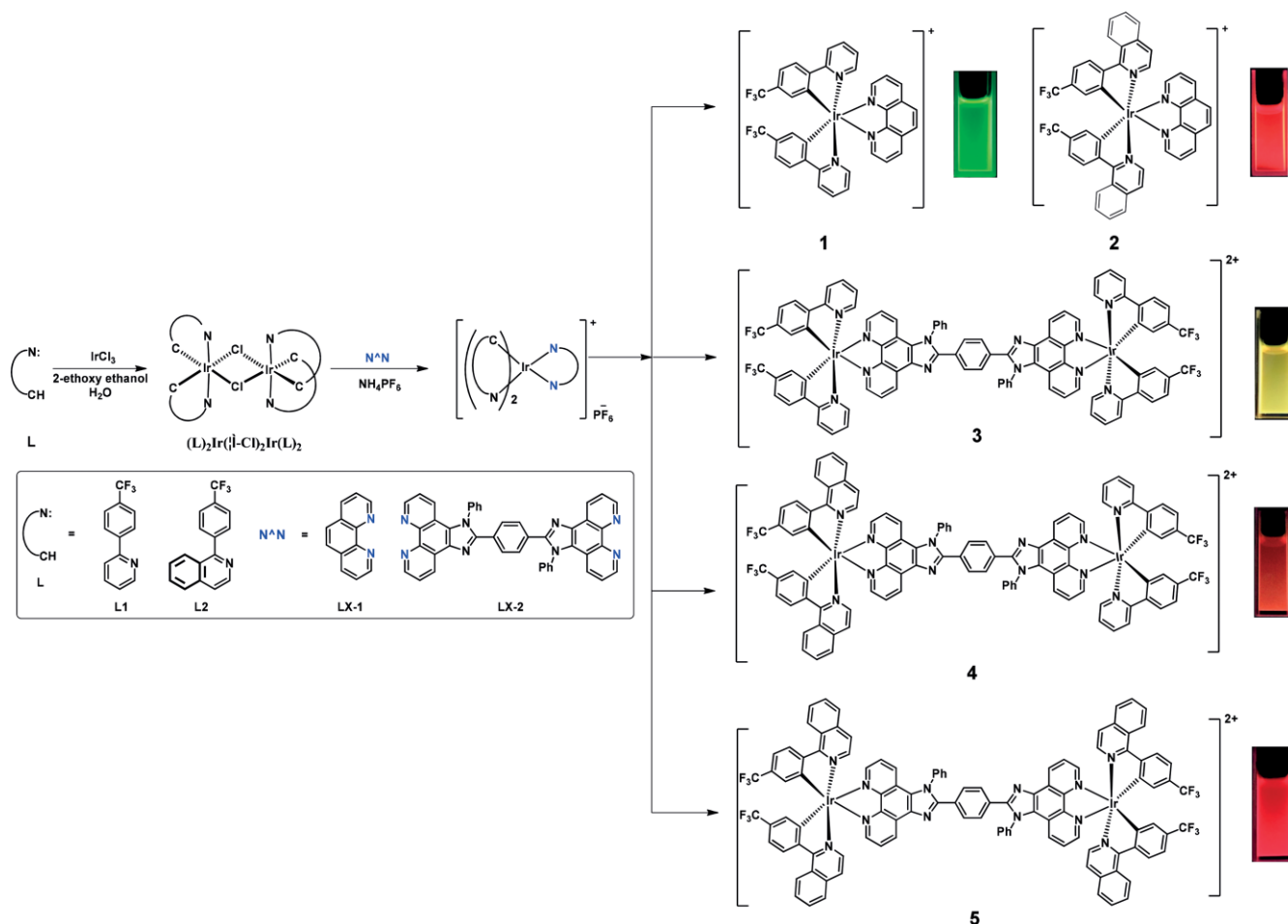
At the end of the molecule, the planar-fused phenanthroline and the adjacent five-membered ring (C26-N5-C27-C28-N6, C11-C12-N1-C13-N2) are almost coplanar with the average deviation from a least-squares plane of 0.0183 Å and 0.0211 Å, respectively. In the center of the molecule, the benzene ring (C20-C21-C22-C23-C24-C25) is slightly twisted with respect to the two five-membered rings, and the dihedral angles are 34.39° and 36.25°, respectively. In addition, the other two benzene rings (C14-C15-C16-C17-C18-C19 and C29-C30-C31-C32-C33-C34) are largely twisted relative to their connected five-membered rings with the dihedral angles of 73.48° and 71.85°, respectively. The crystal packing diagram (Figure 1b) shows a strong face-to-face π -stacking interaction (3.679 Å) between the pyridine ring and the phenyl ring of different phenanthroline groups in two neighbouring molecules. These intramolecular head-to-tail π - π stacking interactions may explain the relatively poor emission in dinuclear complexes.^[21,23]

Electronic Absorption Spectra

The UV-vis absorption of complexes **1–5** in CH_2Cl_2 solution at room temperature are compared in Figure 2 and the data are compiled in Table 1. All five complexes exhibit intense bands in the UV region (<300 nm), which are assigned to spin-allowed singlet ligand-centered (1LC) electronic transitions. The weaker bands which extend to 450 nm are ascribed to both metal-to-ligand (MLCT) and ligand-to-ligand (LLCT) transitions following literature precedents.^[33,34] Clearly, the absorption spectra of mononuclear complexes **1** and **2** are different (Figure 2a), while the spectra of the dinuclear complexes **3**, **4** and **5** are similar (Figure 2b). For the first series, compared to complex **1**, complex **2** displays a significant red-shift in the lowest-energy absorption



Scheme 1. Synthetic routes of ligands **L1–L2** and **LX-2**.



Scheme 2. Synthetic routes of Ir(III) complexes **1–5**.

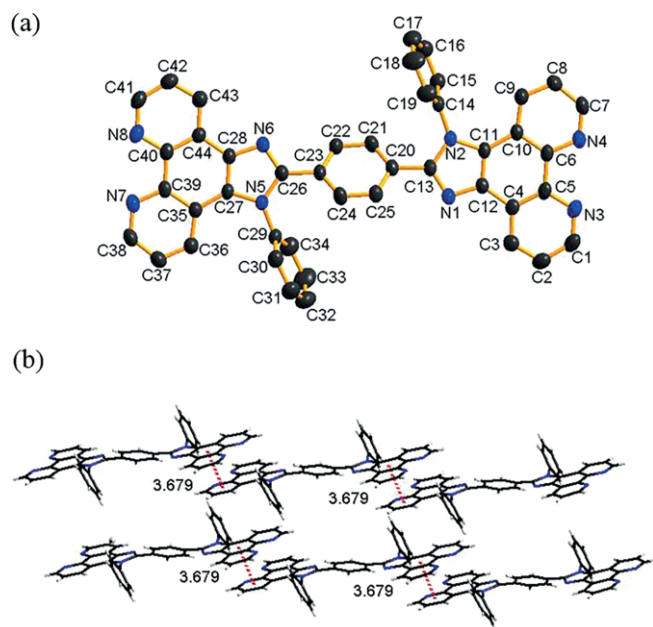


Figure 1. (a) The X-ray molecular structure of **LX-2**. The H atoms are omitted for clarity. (b) The π - π packing diagram of **LX-2**. Selected interactions are depicted as red dotted line.

region, resulting from the more extended π -conjugation of the $C^{\wedge}N$ ligands.^[35] For the second series, the trend of the absorption onset is **3**<**4**<**5**, similar to that observed for **1–2**. This further proves the fact that expanding the conjugation system is favorable for the red shift in spectra.^[26,36] To probe the nature of the low-lying transitions in these complexes, we have performed DFT calculation studies involving the frontier orbital analyses and the main transitions.

Theoretical Calculations

The most representative molecular frontier orbital diagrams for these complexes and the energy gap are presented in Figure 3. The calculated spin-allowed electronic transitions are provided in Table 2, as well as compared with the experimental absorption spectra data. The electron density distributions are summarized in Table S3. Especially, the bridge centre in diiridium complexes **3–5** is considered ancillary ligand.

In general, the HOMOs are primarily localized on the iridium centers and the cyclometalated ligands (Figure 3), corroborating the later investigated electrochemical behavior. However, the HOMO-2 of complex **3** is located on the bridging ancillary ligands. On the other hand, the LUMOs are based largely on the phenanthroline moieties of bridging ancillary ligands, while

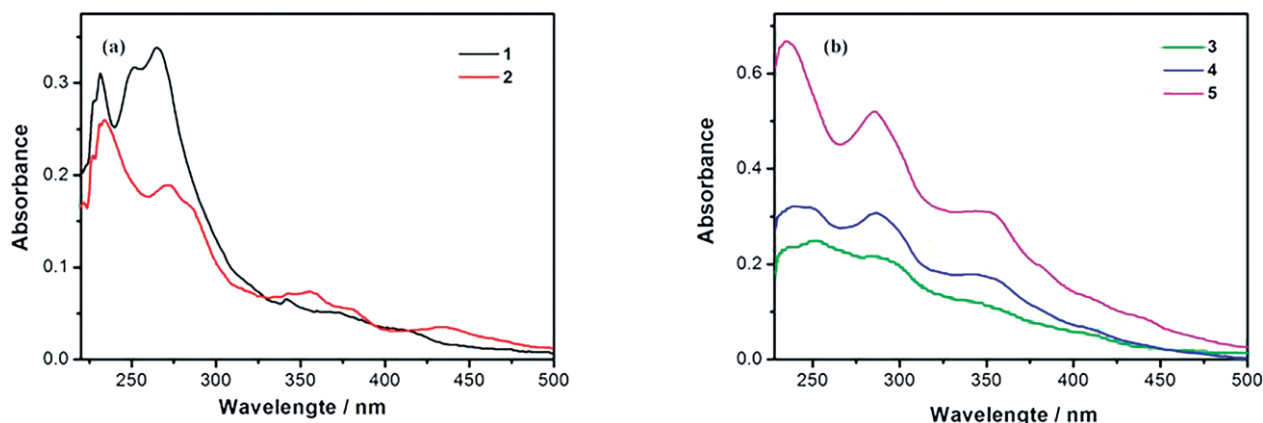


Figure 2. Absorption spectra of (a) 1–2 and (b) 3–5 in CH₂Cl₂ solution.

Table 1. Photophysical and electrochemistry data of complexes 1–5.

Complex	Absorption λ_{obs} [nm] ^[a]	Emission		Φ_{PL} [%] ^[b]	τ [μ s] ^[a]	k_r (10^5 s ⁻¹) ^[c]	k_{nr} (10^5 s ⁻¹) ^[c]	λ_{solid}^{em} [nm] ^[d]	Electrochemistry	
		$\lambda_{em}^{solution}$ [nm] ^[a]	λ_{em}^{solid} [nm] ^[d]						E_{ox} (V) ^[e]	ΔE (V) ^[f]
1	228, 231, 251, 265, 341, 368, 408	519	519	93.5	1.66	5.63	0.39	524, 539	1.60	–
2	227, 231, 234, 272, 286, 341, 358, 380, 435	596	596	37.2	2.57	1.45	2.44	615	1.59	–
3	236, 250, 285, 339, 409	536	536	61.7	2.89	2.13	1.33	554	0.92, 1.62	0.70
4	238, 250, 285, 341, 356, 408, 438	541(sh), 593	541(sh), 593	16.6	2.01	0.83	4.15	598, 624(sh)	0.86, 1.60	0.74
5	234, 285, 348, 409, 441	600	600	27.2	1.67	1.63	4.36	600, 620(sh)	0.81, 1.61	0.80

[a] Data were collected from degassed CH₂Cl₂ solutions at room temperature. [b] *fac*-Ir(ppy)₃ as referenced standard ($\Phi_{PL} = 0.4$).^[37] [c] Radiative decay rate (k_r), nonradiative decay rate (k_{nr}) and pure radiative lifetime (τ_r) estimated from the measured quantum yields and lifetimes. [d] Recorded in solid state at room temperature. [e] Oxidation peak potentials for irreversible processes. [f] Peak splitting between E_{ox1} and E_{ox2} .

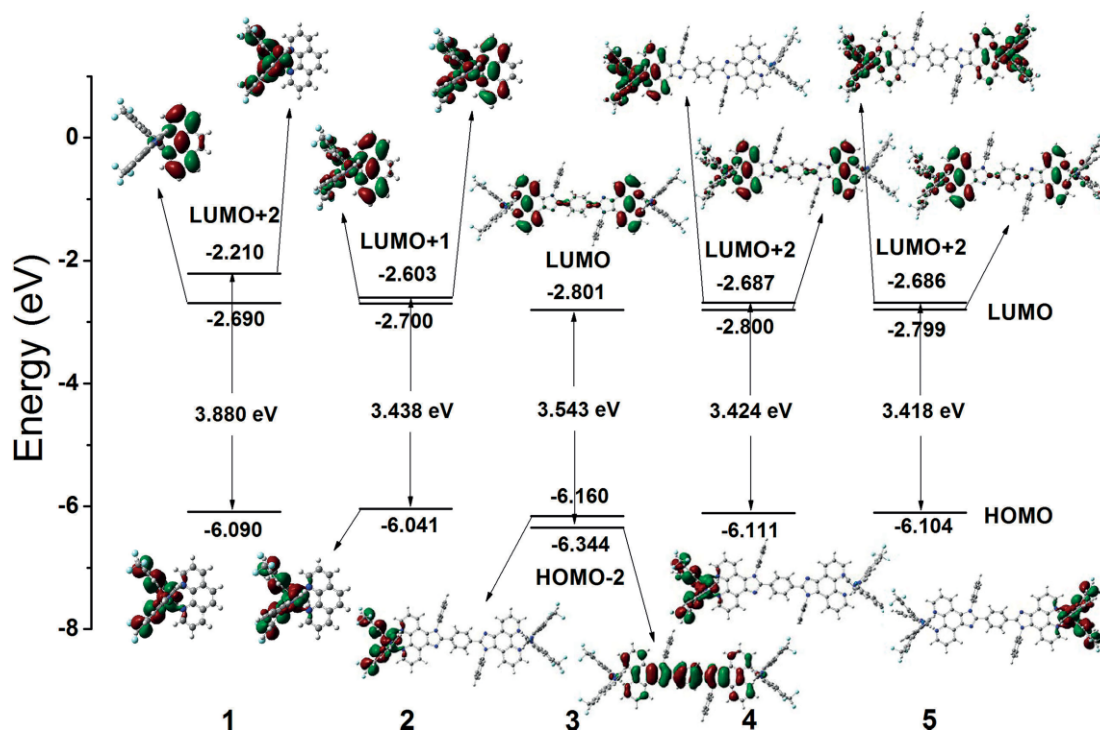


Figure 3. The frontier molecular orbital energy-level diagrams of 1–5 from DFT calculations.

the LUMO+1 of **2** and LUMO+2s of **1**, **4**, **5** mainly reside on the two or four cyclometalated ligands (Figure 3). Therefore, the lowest-energy electronic transitions (HOMO → LUMO+2, HOMO

→ LUMO+1, HOMO-2 → LUMO) are ascribed as MLCT, LLCT and LC transitions (Table 2), which are consistent with the actual absorption and emission.

Table 2. Main experimental and calculated optical transitions for 1–5.

Complex	Orbital Excitations	Primary Character	Oscillation Strength	Calcd [nm]	Exptl [nm]
1	HOMO → LUMO+2	MLCT/LLCT	0.0697	394	408
2	HOMO → LUMO+1	MLCT/LLCT/LC	0.0688	452	435
3	HOMO-2 → LUMO	MLCT/LLCT	0.6760	403	409
4	HOMO → LUMO+2	MLCT/LLCT/LC	0.0732	454	438
5	HOMO → LUMO+2	MLCT/LLCT/LC	0.0717	455	441

From Figure 3, it is found that the more conjugation effect of C[∞]N ligands in **2** and **4–5**, compared to **1** and **3**, can destabilize the HOMOs and stabilize the LUMOs, thereby resulting in much lower transition energies and the red-shifting in absorption and emission. Particularly, in the case of the diiridium complex **5**, the energy gap (3.418 eV, HOMO → LUMO+2) is the smallest one and the absorption wavelength (455 nm) is the longest one in the family of complexes. These results are in good agreement with the photophysical properties discussed in this study. Moreover, the trend in the experimental absorption edge (Table 2) correlates well with the variation rule of the calculated absorption bands, as does the trend in the experimental emission bands below.

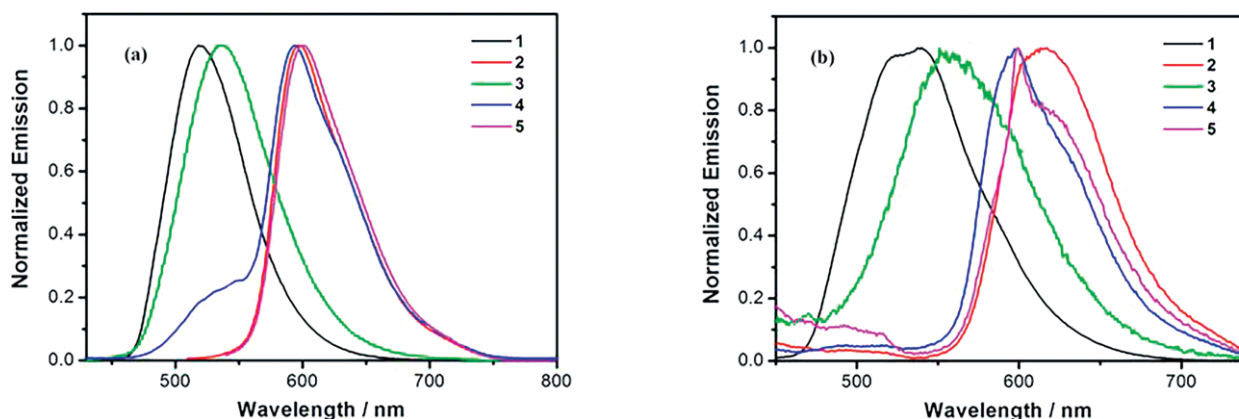
To gain the origins of dual emission for complex **4**, we employed the DFT calculations to investigate the lowest triplet excited states, as well as compared with complexes **1–2**. The spin densities of the triplet states of complexes **1**, **2** and **4** are shown in Figure S1. The corresponding calculated emission energies are summarized in Table S4. For the triplet state of complex **4**, two distinct minima (**T_{1a}** and **T_{1b}**) are found. Moreover, **T_{1a}** is localized at the piq-based side, while **T_{1b}** at the ppy-based side, similar with the triplet states of **2** and **1**, respectively (see Figure S1). Thus, the experimental values of 541 nm and 593 nm are attributed to the ³LLCT/³ML_{ppy}CT and ³LC/³ML_{piq}CT emission, respectively.

As shown in Table S4, the emission peak of complex **1** and the higher energy emission peak of complex **4** are well reproduced by TDDFT. However, the calculation results for the emission peak of complex **2** and the lower energy emission peak of complex **4** do not agree well with the experimental ones. The disagreement between calculation and experiment can be ascribed to the systematic problem of TDDFT method for these

singlet-triplet transitions.^[38] When Tamm–Dancoff approximation (TDA)^[39] is used, the calculation results come much close to the experimental values (see Table S4).

Emission Properties

Upon photoexcitation, all of the complexes described in this study are luminescent in degassed CH₂Cl₂ solution at room temperature (Figure 4a). The corresponding data are also summarized in Table 1. Complexes **1**, **2**, **3** and **5** show broad unstructured emission bands indicative of a predominately ³MLCT state, whereas complex **4** exhibits dual photoluminescence^[40–42] originating from mixed ³LLCT/³ML_{ppy}CT and ³LC/³ML_{piq}CT states, as evidenced in above theoretical calculations. The emission maxima for **1–5** are in the order 519, 596, 536, 593 and 600 nm, respectively. Within the two series, the emission bands undergo a red shift in the sequence **1**<**2** and **3**<**4**<**5**, mirroring the trend observed in absorption. In addition, a red-shifting of ca. 17 and 4 nm for the emission maxima is detected when passing from the mono- to dinuclear iridium complexes, **1**→**3** and **2**→**5**, respectively, which in agreement with the previous reports.^[22–24] Consequently, the emission energy of diiridium complex **5** with more extended π-conjugation system is shifted deeper into the expected red region (λ_{em} = 600 nm), as TD-DFT results clearly indicate. For solid state emissions (Figure 4b), there is a similar trend of luminescence bands with solution state emissions, that is **1**<**2** and **3**<**4**<**5**. Interestingly, however, the emission band of **2** is larger than **5**, probably arising from relatively more π–π stacking interactions in the solid state. It can be seen from Table 1 that obviously, all of these complexes have a stronger bathochromic effect and broader

Figure 4. Normalized emission spectra of 1–5 in degassed CH₂Cl₂ solution (a) and solid state (b) at room temperature.

emission than those in the solution state, which is quite typical of solid emission feature.^[43,44]

For all the cases, the luminescence quantum yields in solution at room temperature are estimated to be 16.6–93.5 %. It is noteworthy that the quantum yields of red emitters (**2**, **4**, **5**) are remarkably lower than those of other color complexes, in line with the energy-gap law.^[45–47] And, not surprisingly, diiridium complexes **3** and **5** show much lower quantum yield values relative to monoiridium species **1** and **2**, respectively. Subsequently, their degassed lifetimes (τ) were measured at room temperature, ranging from 1.66 to 2.89 μ s (Table 1), which indicated that the emissive excited states have triplet characters.^[12] The radiative and nonradiative rate constants can be calculated through the equations $k_r = \Phi/\tau$ and $k_{nr} = (1 - \Phi)/\tau$ ^[48] (see Table 1). It is evident that the brightest emission for complex **1** is mainly attributed to the largest k_r value and the smallest k_{nr} value. For red-emitting dinuclear complexes **4–5**, the relatively weak emission is dominated by large nonradiative decay (k_{nr}), caused by energy gap law.

Electrochemical Properties

Electrochemical studies of complexes **1–5** were performed in acetonitrile (Figure 5) and their redox potentials are summarized in Table 1. Complexes **1–2** exhibit an irreversible single-electron-oxidation peak around 1.59–1.60 V, attributed to the Ir(III)/Ir(IV) redox couple with a contribution from cyclometalated fragments, as already evidenced by DFT calculations (Table S3). Complexes **3–5** display two irreversible oxidation peaks, which are assigned to sequential oxidation of each iridium center. The relatively large peak splittings ($\Delta E = 0.70$ – 0.80 V) between the two oxidation processes indicate a weak electronic coupling between the two iridium atoms through the long conjugated bridging units.^[49,19] When the cyclometalated ligands in the two series of complexes are altered, the trend of the oxidation potentials is **1** > **2** and **3** > **4** > **5** (Table 1), while the order of the HOMO energy levels is **1** < **2** and **3** < **4** < **5** (Table 2). The findings suggest that more extended π -conjugation on the C^N ligands can enrich the electron densities and improve the HOMO energy. In addition, the similar changing rule in the oxidation potentials of the two series indicates that the contribution

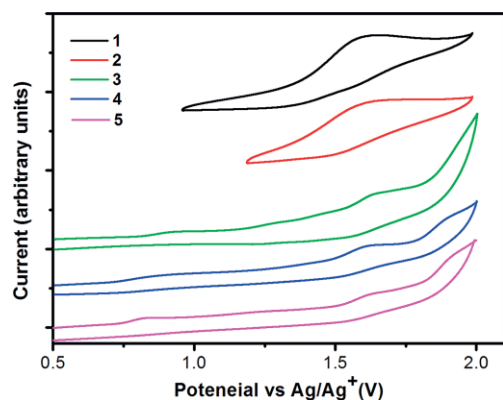


Figure 5. Cyclic voltammograms for complexes **1–5** in CH_3CN solution containing $n\text{-Bu}_4\text{NClO}_4$ (0.1 M) at a sweep rate of 100 mV/s.

of the conjugated bridging units in the dinuclear iridium complexes to the HOMO levels is negligible, which is correlate with the DFT predictions earlier.

Conclusion

Herein, we report two mononuclear $\text{cf}_3\text{ppy}/\text{cf}_3\text{piq}$ -based iridium(III) complexes (**1–2**) and three dinuclear $\text{cf}_3\text{ppy}/\text{cf}_3\text{piq}$ -based iridium(III) complexes (**3–5**) with the same bridging biphen ligand (**LX-2**). Their photophysical properties, theoretical calculations and electrochemical behaviors have been investigated. All Ir(III) complexes are very brightly luminescent with high emission quantum yields and short phosphorescence lifetimes in solution at room temperature. Their phosphorescent colors can be tuned from green to red through either extending π -conjugation system or introducing a second iridium ion. The spectroscopic and redox characterisation of these complexes are complemented by DFT and TD-DFT calculations, supporting the assignment of ${}^3\text{MLCT}/{}^3\text{LLCT}/{}^3\text{LC}$ to the emissive character. We also present that π -conjugation bridges can allow electronic interaction between the two metal centers, causing a red-shift of absorption and emission spectra. Thus, the dinuclearization strategy is an effective pathway for obtaining highly efficient red materials.

Experimental Section

General Information and Materials

All reactions were performed under a nitrogen atmosphere, and all reagents were purchased and used without further purification unless otherwise stated. ${}^1\text{H}$, ${}^{19}\text{F}$ and ${}^{31}\text{P}$ spectra were recorded on a Bruker AM 400 MHz instrument, and chemical shifts were reported in ppm relative to Me_4Si as an internal standard. ESI-MS spectra were performed on a Bruker esquire HCT-Agilent 1200 spectrometer. Elemental analyses were performed on a Vario EL Cube Analyzer system at Hainan Normal University. UV-vis spectra were recorded on a Hitachi U3900/3900H spectrophotometer. Fluorescence spectra were carried out on a Hitachi F-7000 spectrophotometer as deaerated CH_2Cl_2 solutions at room temperature, as well as for the neat solid powders. Luminescence lifetime curves were measured on an Edinburgh Instruments FLS920P fluorescence spectrometer and the data were treated as one-order exponential fitting using OriginPro 8 software.

Synthetic Procedures

Synthesis of 2-(4-(trifluoromethyl)phenyl)pyridine (cf_3ppy , **L1**) To a solution of 2-bromopyridine (1.13 g, 7.15 mmol), (Trifluoromethyl)phenylboronic acid (1.50 g, 7.90 mmol), 2 mol/L K_2CO_3 (2 mL) in 1,4-dioxane (20 mL), was added $\text{Pd}(\text{dppf})\text{Cl}_2$ (110 mg) as the catalyst, and the mixture was heated at 90 $^\circ\text{C}$ for 12 hours under N_2 . After the solvent was removed, H_2O (50 mL) and ethyl acetate (50 mL) were added. The organic phase was washed with brine and dried with Na_2SO_4 . After concentrated, the residue was purified by flash column chromatography (petroleum ether/ethyl acetate = 50:1) to obtain **L1** (1.35 g, yield: 84.6 %) as a white solid. ${}^1\text{H}$ NMR (400 MHz, CDCl_3) δ (ppm) 8.72 (d, $J = 4.0$ Hz, 1H), 8.11 (d, $J = 8.0$ Hz, 2H), 7.72–7.82 (m, 4H), 7.26–7.31 (m, 1H). MS (ESI): m/z 223.13 [$\text{M} + \text{H}$]⁺ (calcd 223.06).

Synthesis of 1-(4-(trifluoromethyl)phenyl)isoquinoline (cf_3piq , **L2**) A procedure analogous to that described for **L1** was used with 1-

chloroisoquinoline instead of 2-bromopyridine to afford **L2** as a white solid. (0.85 g, yield: 81.7 %). ¹H NMR (400 MHz, CDCl₃) δ (ppm) 8.63 (d, *J* = 5.7 Hz, 1H), 8.02 (d, *J* = 8.5 Hz, 1H), 7.92 (d, *J* = 8.2 Hz, 1H), 7.79–7.84 (m, 4H), 7.70–7.74 (m, 2H), 7.55–7.59 (m, 1H). MS (ESI): *m/z* 273.16 [M + H]⁺ (calcd 273.08).

Synthesis of 1,4-bis(1-phenyl-1H-imidazo[4,5-f][1,10]phenanthroline-2-yl)benzene (biphen, **LX-2**) 1,10-phenanthroline-5,6-dione (500 mg, 2.38 mmol), aniline (222 mg, 2.38 mmol), terephthalaldehyde (160 mg, 1.19 mmol) and NH₄Ac (2.93 g, 47.58 mmol) were mixed into acetic acid (25 mL) and heated at 130 °C for 24 hours under N₂. After cooled to room temperature, the mixture was poured to ice water and used 25 % ammonia solution to adjust the pH to neutral. The solid was filtered, dried and recrystallized from methanol to afford a brown solid **LX-2** (0.76 g, 48.23 %). ¹H NMR (400 MHz, CDCl₃) δ (ppm) 9.12–9.16 (m, 2H), 9.07–9.15 (m, 2H), 9.05 (d, *J* = 2.8 Hz, 2H), 7.75 (dd, *J* = 8.1, 4.4 Hz, 3H), 7.61–7.71 (m, 6H), 7.48–7.57 (m, 7H), 7.43 (d, *J* = 7.1 Hz, 2H), 7.30 (dd, *J* = 8.4, 4.3 Hz, 2H). MS (ESI): *m/z* 666.18 [M + H]⁺ (calcd 666.23).

General synthetic procedure for Ir(III) complexes 1–5.

Synthesis of the mononuclear Ir(III) complexes (**1**, **2**)

The cyclometalated Ir(III) dichloro-bridged dimers [(C[^]N)₂Ir(μ-Cl)]₂, were synthesized by IrCl₃·3H₂O with 2.2 equiv of the ligand **L1** or **L2** in a 3:1 mixture of 2-ethoxyethanol and deionized water according to a similar method reported by Nonoyama.^[32] And then the mononuclear Ir(III) complexes **1** and **2** were prepared by the reaction of Ir(III) dichloro-bridged dimers with 2.5 equiv of 1,10-phenanthroline (**LX-1**) in DCM and MeOH (v:v = 2:1) and heated at 40 °C for 5 hours under nitrogen atmosphere. After the reaction was completed, NH₄PF₆ (5.0 equiv.) was added and the reaction mixture was stirred at room temperature for 3 hours. The reaction mixture was diluted with water and extracted multiple times with DCM. The combined organic phase was concentrated and the residue was purified by column chromatography (DCM/MeOH = 100:1) to afford pure complexes **1** and **2**.

Complex **1** (48 mg, yield: 82.5 %), yellow solid. ¹H NMR (400 MHz, DMSO) δ (ppm) 8.93 (dd, *J* = 8.3, 1.3 Hz, 2H), 8.46 (d, *J* = 8.1 Hz, 2H), 8.41 (s, 2H), 8.18–8.22 (m, 4H), 8.00–8.08 (m, 4H), 7.60 (d, *J* = 5.1 Hz, 2H), 7.42 (dd, *J* = 8.1, 1.2 Hz, 2H), 7.13–7.16 (m, 2H), 6.42 (d, *J* = 1.2 Hz, 2H). ¹⁹F NMR (377 MHz, DMSO) δ (ppm) –61.31 (s, 3F, CF₃), –69.18 (s, 3F, PF₆), –71.07 (s, 3F, PF₆). ³¹P NMR (162 MHz, DMSO) δ (ppm) –144.20 (hept, PF₆). MS (ESI): *m/z* 817.04 [M – PF₆]⁺ (calcd 817.14). Anal. Calcd for C₃₆H₂₂F₁₂IrN₄P: C, 44.96; H, 2.31; N, 5.83 %; found C, 44.93; H, 2.34; N, 5.86 %.

Complex **2** (52 mg, yield: 81.6 %), red solid. ¹H NMR (400 MHz, DMSO) δ (ppm) 9.02–9.05 (m, 2H), 8.93 (dd, *J* = 8.3, 1.3 Hz, 2H), 8.61 (d, *J* = 8.5 Hz, 2H), 8.42 (s, 2H), 8.09–8.17 (m, 4H), 8.04 (dd, *J* = 8.2, 5.1 Hz, 2H), 7.87–7.91 (m, 4H), 7.60 (d, *J* = 6.4 Hz, 2H), 7.46–7.50 (m, 4H), 6.42 (s, 2H). ¹⁹F NMR (377 MHz, DMSO) δ (ppm) –61.77 (s, 3F, CF₃), –69.20 (s, 3F, PF₆), –71.09 (s, 3F, PF₆). ³¹P NMR (162 MHz, DMSO) δ (ppm) –144.20 (hept, PF₆). MS (ESI): *m/z* 917.08 [M – PF₆]⁺ (calcd 917.17). Anal. Calcd for C₄₄H₂₆F₁₂IrN₄P: C, 49.77; H, 2.47; N, 5.28 %; found C, 49.79; H, 2.43; N, 5.29 %.

Synthesis of the binuclear Ir(III) complexes (**3**, **5**)

A mixture of the Ir(III) dichloro-bridged dimers [(C[^]N)₂Ir(μ-Cl)]₂ (100 mg) and the ancillary ligand **LX-2** (1.1 equiv.) was dissolved in 6 mL of DCM and MeOH (v:v = 2:1), and heated at 40 °C for 10 hours under nitrogen atmosphere. After this time, the reaction mixture was cooled to room temperature and NH₄PF₆ (8.0 equiv.) was added. The mixture was stirred at room temperature for 5 hours. The mixture was diluted with water and extracted multiple times

with DCM. The combined organic phase was concentrated and the residue was purified by column chromatography (DCM/MeOH = 50:1) to afford the binuclear Ir(III) complexes **3** and **5**.

Complex **3** (43 mg, yield: 29.8 %), yellow solid. ¹H NMR (400 MHz, DMSO) δ (ppm) 9.34 (d, *J* = 7.2 Hz, 2H), 8.45–8.51 (m, 4H), 8.19–8.24 (m, 8H), 8.03–8.07 (m, 6H), 7.73–7.80 (m, 13H), 7.54–7.64 (m, 7H), 7.55 (d, *J* = 8.3 Hz, 2H), 7.39–7.45 (m, 4H), 7.17 (t, *J* = 6.4 Hz, 4H), 6.39–6.43 (m, 4H). ¹⁹F NMR (377 MHz, DMSO) δ (ppm) –61.32 (s, 3F, CF₃), –61.33 (s, 3F, CF₃), –69.21 (s, 3F, PF₆), –71.09 (s, 3F, PF₆). ³¹P NMR (162 MHz, DMSO) δ (ppm) –144.29 (hept, PF₆). MS (ESI): *m/z* 1940.23 [M – PF₆]⁺ (calcd 1940.37). Elemental anal. calcd. for C₉₂H₅₄F₂₄Ir₂N₁₂P₂: C, 49.55; H, 2.44; N, 7.54 %; found C, 49.53; H, 2.46; N, 7.58 %.

Complex **5** (38 mg, yield: 27.4 %), red solid. ¹H NMR (400 MHz, CDCl₃) δ (ppm) 9.32–9.35 (m, 2H), 9.00–9.08 (m, 4H), 8.62 (dd, *J* = 15.0, 8.4 Hz, 4H), 8.12–8.16 (m, 7H), 7.94–8.02 (m, 10H), 7.77–7.84 (m, 14H), 7.62–7.64 (m, 6H), 7.47–7.57 (m, 10H), 6.44 (s, 2H), 6.37 (s, 2H). ¹⁹F NMR (377 MHz, DMSO) δ (ppm) –61.76 (s, 3F, CF₃), –61.82 (s, 3F, CF₃), –69.20 (s, 3F, PF₆), –71.09 (s, 3F, PF₆). ³¹P NMR (162 MHz, DMSO) δ (ppm) –144.29 (hept, PF₆). MS (ESI): *m/z* 2140.33 [M – PF₆]⁺ (calcd 2140.43). Elemental anal. calcd. for C₁₀₈H₆₂F₂₄Ir₂N₁₂P₂: C, 53.38; H, 2.57; N, 6.92 %; found C, 53.41; H, 2.56; N, 6.90 %.

Synthesis of the binuclear Ir(III) complex **4**

To a solution of the ancillary ligand **LX-2** (2.2 equiv.) in 6 mL of DCM and MeOH (v:v = 2:1) at 40 °C under nitrogen atmosphere, was added the Ir(III) dichloro-bridged dimer [(L₁)₂Ir(μ-Cl)]₂ (100 mg) in three portions. The reaction mixture was stirred at this temperature for 3 hours. After this time, the Ir(III) dichloro-bridged dimer [(L₂)₂Ir(μ-Cl)]₂ (1.0 equiv.) was added and stirred for another 5 hours. After the reaction mixture was cooled to room temperature, NH₄PF₆ (8.0 equiv.) was added and the mixture was stirred at room temperature for 8 hours. The reaction mixture was diluted with water and extracted multiple times with DCM. The combined organic phase was concentrated and the residue was purified by column chromatography (DCM/MeOH = 50:1) to afford the binuclear Ir(III) complex **4**.

Complex **4** (36 mg, yield: 27.3 %), red solid. ¹H NMR (400 MHz, DMSO) δ (ppm) 9.34 (d, *J* = 8.0 Hz, 2H), 9.02–9.05 (m, 2H), 8.62 (dd, *J* = 15.0, 8.6 Hz, 2H), 8.47 (dd, *J* = 14.8, 8.3 Hz, 2H), 8.14–8.24 (m, 8H), 8.01–8.08 (m, 4H), 7.93–7.96 (m, 4H), 7.72–7.80 (m, 13H), 7.60–7.63 (m, 7H), 7.52–7.57 (m, 5H), 7.39–7.43 (m, 4H), 7.17 (t, *J* = 6.4 Hz, 2H), 6.37–6.45 (m, 4H). ¹⁹F NMR (377 MHz, DMSO) δ (ppm) –61.32 (s, 3F, CF₃), –61.33 (s, 3F, CF₃), –61.76 (s, 3F, CF₃), –61.82 (s, 3F, CF₃), –69.21 (s, 3F, PF₆), –71.10 (s, 3F, PF₆). ³¹P NMR (162 MHz, DMSO) δ (ppm) –144.20 (hept, PF₆). MS (ESI): *m/z* 2040.35 [M – PF₆]⁺ (calcd 2040.40). Elemental anal. calcd. for C₁₀₀H₅₈F₂₄Ir₂N₁₂P₂: C, 51.55; H, 2.51; N, 7.21 %; found C, 51.57; H, 2.50; N, 7.20 %.

X-ray Structure Determination. X-ray diffraction data were collected with an Agilent Technologies Gemini A Ultra diffractometer equipped with graphite-monochromated Mo-K_α radiation (λ = 0.7107 Å) at room temperature. Data collection and reduction were processed with CrysAlisPro software.^[50] All of the structures were solved using Superflip^[51] and refined using SHELXL-2014^[52] within Olex2.^[53] All non-hydrogen atoms were found in alternating difference Fourier syntheses and least-squares refinement cycles and, during the final cycles, refined anisotropically. Hydrogen atoms were placed in calculated positions and refined as riding atoms with a uniform value of *U*_{iso}.

CCDC 1876931 (for **LX-2**) contains the supplementary crystallographic data for this paper. These data can be obtained free of charge from The Cambridge Crystallographic Data Centre.

Electrochemical Measurements. Cyclic voltammetry (CV) was performed on a CHI 1210B electrochemical workstation, with a glassy carbon electrode as the working electrode, a platinum wire as the counter electrode, an Ag/Ag⁺ electrode as the reference electrode, and 0.1 M *n*-Bu₄NClO₄ as the supporting electrolyte.

Computational Details. All calculations were carried out with Gaussian 09 software package.^[54] The density functional theory (DFT) and time-dependent DFT (TDDFT) were employed with no symmetry constraints to investigate the optimized geometries and electron configurations with the Becke three-parameter Lee-Yang-Parr (B3LYP) hybrid density functional theory.^[55–57] Unrestricted DFT method was used to optimize the triplet state geometries. The LANL2DZ basis set was used to treat the Ir atom, whereas the 6–31G* basis set was used to treat C, H, N and F atoms. Solvent effects were considered within the SCRf (self-consistent reaction field) theory using the polarized continuum model (PCM) approach to model the interaction with the solvent.^[58,59]

Acknowledgments

This work was supported by the National Natural Science Foundation of China (21501037), the Natural Science Foundation of Hainan Province (218QN236), the 2017 Hainan Normal University's Innovation Experiment Program for University Students-China and Program for Innovative Research Team in University (IRT-16R19).

Keywords: Iridium · Dinuclear complexes · Conjugated ligands · Phosphorescence

- [1] Y. S. Li, J. L. Liao, K. T. Lin, W. Y. Hung, S. H. Liu, G. H. Lee, P. T. Chou, Y. Chi, *Inorg. Chem.* **2017**, *56*, 10054–10060.
- [2] K. T. Kamtekar, A. P. Monkman, M. R. Bryce, *Adv. Mater.* **2010**, *22*, 572–582.
- [3] K. K. W. Lo, M. W. Louie, K. Y. Zhang, *Coord. Chem. Rev.* **2010**, *254*, 2603–2622.
- [4] L. Flamigni, A. Barbieri, C. Sabatini, B. Ventura, F. Barigelletti, *Top. Curr. Chem.* **2007**, *281*, 143–203.
- [5] E. Baranoff, E. Orselli, L. Allouche, D. DiCenso, R. Scopelliti, M. Grätzl, M. K. Nazeeruddin, *Chem. Commun.* **2011**, *47*, 2799–2801.
- [6] M. A. Baldo, M. E. Thompson, S. R. Forrest, *Nature* **2000**, *403*, 750–753.
- [7] E. Matteucci, A. Baschieri, A. Mazzanti, L. Sambri, J. Avila, A. Pertegas, H. J. Bolink, F. Monti, E. Leoni, N. Armadori, *Inorg. Chem.* **2017**, *56*, 10584–10595.
- [8] T.-Y. Li, J. Wu, Z.-G. Wu, Y.-X. Zheng, J.-L. Zuo, Y. Pan, *Coord. Chem. Rev.* **2018**, *374*, 55–92.
- [9] A. F. Henwood, E. Zysman-Colman, *Chem. Commun.* **2017**, *53*, 807–826.
- [10] Y.-J. Cho, S.-Y. Kim, C. M. Choi, N. J. Kim, C. H. Kim, D. W. Cho, H.-J. Son, C. Pac, S. O. Kang, *Inorg. Chem.* **2017**, *56*, 5305–5315.
- [11] B. Balónová, D. R. Martir, E. R. Clark, H. J. Shepherd, E. Zysman-Colman, B. A. Blight, *Inorg. Chem.* **2018**, *57*, 8581–8587.
- [12] S. Bettington, M. Tavasli, M. R. Bryce, A. S. Batsanov, A. L. Thompson, H. A. Al-Attar, F. B. Dias, A. P. Monkman, *J. Mater. Chem.* **2006**, *16*, 1046–1052.
- [13] X. Li, D. Zhang, W. Li, B. Chu, L. Han, T. Li, Z. Su, J. Zhu, Y. Chen, Z. Hu, P. Lei, Z. Zhang, *Opt. Mater.* **2009**, *31*, 1173–1176.
- [14] A. Auffrant, A. Barbieri, F. Barigelletti, J. Lacour, P. Mobian, J.-P. Collin, J.-P. Sauvage, B. Ventura, *Inorg. Chem.* **2007**, *46*, 6911–6919.
- [15] Y. Zheng, A. S. Batsanov, M. A. Fox, H. A. Al-Attar, K. Abdullah, V. Jankus, M. R. Bryce, A. P. Monkman, *Angew. Chem. Int. Ed.* **2014**, *53*, 11616–11619; *Angew. Chem.* **2014**, *126*, 11800.
- [16] R. E. Daniels, S. Culham, M. C. Hunter, M. R. Probert, W. Clegg, J. A. G. Williams, V. N. Kozhevnikov, *Dalton Trans.* **2016**, *45*, 6949–6962.
- [17] V. W.-W. Yam, K. M.-C. Wong, *Chem. Commun.* **2011**, *47*, 11579–11592.
- [18] P.-H. Lanoë, C. M. Tong, R. W. Harrington, M. R. Probert, W. Clegg, J. A. G. Williams, V. N. Kozhevnikov, *Chem. Commun.* **2014**, *50*, 6831–6834.
- [19] D. G. Congrave, Y.-T. Hsu, A. S. Batsanov, A. Beeby, M. R. Bryce, *Dalton Trans.* **2018**, *47*, 2086–2098.
- [20] G. Li, D. G. Congrave, D. Zhu, Z. Su, M. R. Bryce, *Polyhedron* **2018**, *140*, 146–157.
- [21] X. Yang, X. Xu, J. S. Dang, G. Zhou, C. L. Ho, W. Y. Wong, *Inorg. Chem.* **2016**, *55*, 1720–1727.
- [22] F. Lafolet, S. Welter, Z. Popović, L. De Cola, *J. Mater. Chem.* **2005**, *15*, 2820–2828.
- [23] L. Donato, C. E. McCusker, F. N. Castellano, E. Zysman-Colman, *Inorg. Chem.* **2013**, *52*, 8495–8504.
- [24] G. Li, Y. Wu, G. Shan, W. Che, D. Zhu, B. Song, L. Yan, Z. Sua, M. R. Bryce, *Chem. Commun.* **2014**, *50*, 6977–6980.
- [25] V. Chandrasekhar, S. M. W. Rahaman, T. Hajra, D. Das, T. Ghatak, S. Rafiq, P. Sen, J. K. Bera, *Chem. Commun.* **2011**, *47*, 10836–10838.
- [26] G.-N. Li, Y. Zou, Y.-D. Yang, J. Liang, F. Cui, T. Zheng, H. Xie, Z.-G. Niu, *J. Fluoresc.* **2014**, *24*, 1545–1552.
- [27] G.-N. Li, S.-B. Dou, T. Zheng, X.-Q. Chen, X.-H. Yang, S. Wang, W. Sun, G.-Y. Chen, Z.-R. Mo, Z.-G. Niu, *Organometallics* **2018**, *37*, 78–86.
- [28] Z.-G. Niu, L.-P. Yan, L. Wu, G.-Y. Chen, W. Sun, X. Liang, Y.-X. Zheng, G.-N. Li, J.-L. Zuo, *Dyes Pigm.* **2018**, *162*, 863–871.
- [29] H. J. Bae, J. Chung, H. Kim, J. Park, K. M. Lee, T.-W. Koh, Y. S. Lee, S. Yoo, Y. Do, M. H. Lee, *Inorg. Chem.* **2014**, *53*, 128–138.
- [30] M. Xu, G. Wang, R. Zhou, Z. An, Q. Zhou, W. Li, *Inorg. Chim. Acta* **2007**, *360*, 3149–3154.
- [31] A. E. Wendlandt, S. S. Stahl, *J. Am. Chem. Soc.* **2014**, *136*, 506–512.
- [32] M. Nonoyama, *Bull. Chem. Soc. Jpn.* **1974**, *47*, 767–768.
- [33] P. M. Griffiths, F. Loiseau, F. Puntoriero, S. Serroni, S. Campagna, *Chem. Commun.* **2000**, 2297–2298.
- [34] L. He, J. Qiao, L. Duan, G. Dong, D. Zhang, L. Wang, Y. Qiu, *Adv. Funct. Mater.* **2009**, *19*, 2950–2960.
- [35] Z.-G. Niu, H.-B. Han, M. Li, Z. Zhao, G.-Y. Chen, Y.-X. Zheng, G.-N. Li, J.-L. Zuo, *Organometallics* **2018**, *37*, 3154–3164.
- [36] J. Dai, K. F. Zhou, M. Li, H. Q. Sun, Y. Q. Chen, S. J. Su, X. M. Pu, Y. Huang, Z. Y. Lu, *Dalton Trans.* **2013**, *42*, 10559–10571.
- [37] K. A. King, P. J. Spellane, R. J. Watts, *J. Am. Chem. Soc.* **1985**, *107*, 1431–1432.
- [38] R. Bauernschmitt, R. Ahlrichs, *Chem. Phys. Lett.* **1996**, *256*, 454–464.
- [39] S. Hirata, M. Head-Gordon, *Chem. Phys. Lett.* **1999**, *314*, 291–299.
- [40] D. Escudero, D. Jacquemin, *Dalton Trans.* **2015**, *44*, 8346–8355.
- [41] Y. S. Yeh, Y. M. Cheng, P. T. Chou, G. H. Lee, C. H. Yang, Y. Chi, C. F. Shu, C. H. Wang, *ChemPhysChem* **2006**, *7*, 2294–2297.
- [42] D. Escudero, W. Thiel, *Inorg. Chem.* **2014**, *53*, 11015–11019.
- [43] Q. L. Xu, C. C. Wang, T. Y. Li, M. Y. Teng, S. Zhang, Y. M. Jing, X. Yang, W. N. Li, C. Lin, Y. X. Zheng, J. L. Zuo, X. Z. You, *Inorg. Chem.* **2013**, *52*, 4916–4925.
- [44] Z.-G. Niu, T. Zheng, Y.-H. Su, P.-J. Wang, X.-Y. Li, F. Cui, J. Liang, G.-N. Li, *New J. Chem.* **2015**, *39*, 6025–6033.
- [45] L. F. Gildea, J. A. G. Williams, Iridium and platinum complexes for OLEDs, in *Organic Light-Emitting Diodes: Materials, Devices and Applications*, ed. A. Buckley, Wodhead, Cambridge, **2013**.
- [46] S. C. Lo, E. B. Namdas, P. L. Burn, I. D. W. Samuel, *Macromolecules* **2003**, *36*, 9721–9730.
- [47] E. A. Plummer, J. W. Hofstraat, L. De Cola, *Dalton Trans.* **2003**, 2080–2084.
- [48] B. P. Straughan, S. S. Walker, *Spectroscopy*, 2nd ed.; Chapman and Hall: London, **1976**, Vol. 3.
- [49] V. Chandrasekhar, T. Hajra, J. K. Bera, S. M. W. Rahaman, N. Satumtira, O. Elbjerrami, M. A. Omary, *Inorg. Chem.* **2012**, *51*, 1319–1329.
- [50] CrysAlisPro Version 1.171.36.21. Agilent Technologies Inc. Santa Clara, CA, USA, **2012**.
- [51] L. Palatinus, G. J. Chapuis, *J. Appl. Crystallogr.* **2007**, *40*, 786–790.
- [52] G. M. Sheldrick, *Acta Crystallogr., Sect. A* **2008**, *64*, 112–122.
- [53] O. V. Dolomanov, L. J. Bourhis, R. J. Gildea, J. A. K. Howard, H. J. Puschmann, *J. Appl. Crystallogr.* **2009**, *42*, 339–341.
- [54] M. J. Frisch, G. W. Trucks, H. B. Schlegel, G. E. Scuseria, M. A. Robb, J. R. Cheeseman, G. Scalmani, V. Barone, B. Mennucci, G. A. Petersson, H. Nakatsuji, M. Caricato, X. Li, H. P. Hratchian, A. F. Izmaylov, J. Bloino, G. Zheng, J. L. Sonnenberg, M. Hada, M. Ehara, K. Toyota, R. Fukuda, J. Hasegawa, M. Ishida, T. Nakajima, Y. Honda, O. Kitao, H. Nakai, T. Vreven, J. A.

Montgomery Jr., J. E. Peralta, F. Ogliaro, M. Bearpark, J. J. Heyd, E. Brothers, K. N. Kudin, V. N. Staroverov, R. Kobayashi, J. Normand, K. Raghavachari, A. Rendell, J. C. Burant, S. S. Iyengar, J. Tomasi, M. Cossi, N. Rega, J. M. Millam, M. Klene, J. E. Knox, J. B. Cross, V. Bakken, C. Adamo, J. Jaramillo, R. Gomperts, R. E. Stratmann, O. Yazyev, A. J. Austin, R. Cammi, C. Pomelli, J. W. Ochterski, R. L. Martin, K. Morokuma, V. G. Zakrzewski, G. A. Voth, P. Salvador, J. J. Dannenberg, S. Dapprich, A. D. Daniels, Ö. Farkas, J. B. Foresman, J. V. Ortiz, J. Cioslowski, D. J. Fox, *Gaussian 09, Revision A.01*, Gaussian, Inc., Wallingford CT, **2009**.

[55] C. Lee, W. Yang, R. G. Parr, *Phys. Rev. B* **1988**, *37*, 785–789.

[56] B. Miehlich, A. Savin, H. Stoll, H. Preuss, *Chem. Phys. Lett.* **1989**, *157*, 200–206.

[57] A. D. Becke, *J. Chem. Phys.* **1993**, *98*, 5648–5652.

[58] M. Cossi, N. Rega, G. Scalmani, V. Barone, *J. Comput. Chem.* **2003**, *24*, 669–681.

[59] J. Tomasi, B. Mennucci, R. Cammi, *Chem. Rev.* **2005**, *105*, 2999–3093.

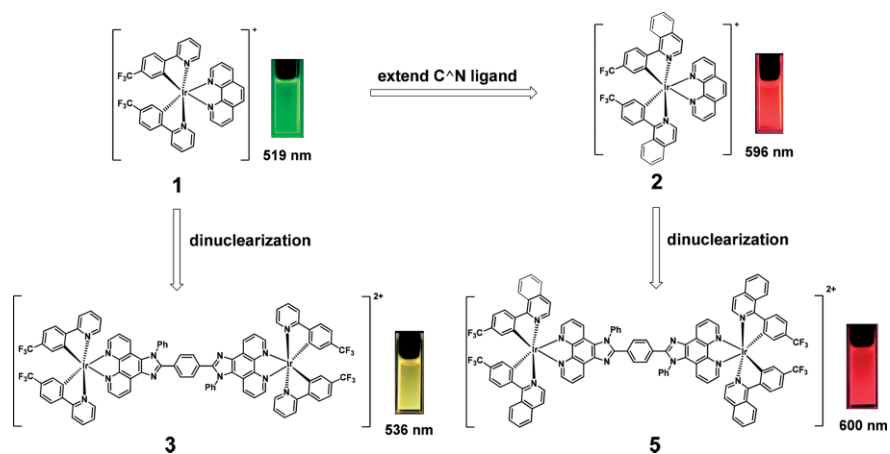
Received: November 7, 2018

Luminescent Iridium(III) Complexes

X.-H. Yang, M. Li, H. Peng, Q. Zhang,
S.-X. Wu, W.-Q. Xiao, X.-L. Chen,
Z.-G. Niu, G.-Y. Chen, G.-N. Li* 1–10



Highly Luminescent Mono- and Di-nuclear Cationic Iridium(III) Complexes Containing Phenanthroline-Based Ancillary Ligand



A new family of mononuclear and di-nuclear $\text{cf}_3\text{ppy}/\text{cf}_3\text{piq}$ -based iridium(III) complexes containing phenanthroline-based ancillary ligands have been synthesized. Their phosphorescent colors

can be tuned from green to red through either extending π -conjugation system or introducing a second iridium ion.

DOI: 10.1002/ejic.201801367